Neuroimage: Reports 4 (2024) 100222

Contents lists available at ScienceDirect

Neuroimage: Reports

journal homepage: www.sciencedirect.com/journal/neuroimage-reports

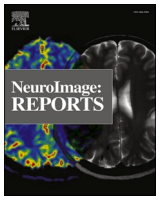

Changes in functional and structural brain connectivity following bilateral hand transplantation

David J. Madden [a,b,*], Jenna L. Merenstein [b], Todd B. Harshbarger [b,c], Linda C. Cendales [d]

[a] Department of Psychiatry and Behavioral Sciences, Duke University Medical Center, Durham, NC, USA
[b] Brain Imaging and Analysis Center, Duke University Medical Center, Durham, NC, USA
[c] Department of Radiology, Duke University Medical Center, Durham, NC, USA
[d] Department of Surgery, Duke University Medical Center, Durham, NC, USA

ARTICLE INFO

Keywords:
Neuroplasticity
Vascularized composite allograft
Amputation

ABSTRACT

As a surgical treatment following amputation or loss of an upper limb, nearly 200 hand transplantations have been completed to date. We report here a magnetic resonance imaging (MRI) investigation of functional and structural brain connectivity for a bilateral hand transplant patient (female, 60 years of age), with a preoperative baseline and three postoperative testing sessions each separated by approximately six months. We used graph theoretical analyses to estimate connectivity within and between modules (networks of anatomical nodes), particularly a sensorimotor network (SMN), from resting-state functional MRI and structural diffusion-weighted imaging (DWI). For comparison, corresponding MRI measures of connectivity were obtained from 10 healthy, age-matched controls, at a single testing session. The patient's within-module functional connectivity (both SMN and non-SMN modules), and structural within-SMN connectivity, were higher preoperatively than that of the controls, indicating a response to amputation. Postoperatively, the patient's within-module functional connectivity decreased towards the control participants' values, across the 1.5 years postoperatively, particularly for hand-related nodes within the SMN module, suggesting a return to a more canonical functional organization. Whereas the patient's structural connectivity values remained relatively constant postoperatively, some evidence suggested that structural connectivity supported the postoperative changes in within-module functional connectivity.

1. Introduction

With evolving techniques in microsurgery, hand transplantation is a viable treatment option following amputation of an upper limb. Hand transplantation is a form of vascularized composite allografts (VCA), or composite tissue allotransplantation, which is transplantation of non-autologous tissues (i.e., skin, muscle, tendon, nerve and bone) as a functional unit to reconstruct defects that cannot be reconstructed with autologous tissues (Cendales et al., 2012; MacKay et al., 2014; Shores et al., 2010, 2017; Wells et al., 2022). Following the first successful hand transplant in 1998 (Dubernard et al., 1999), 148 hand transplants have been performed, worldwide, through 2022 (Wells et al., 2022). This group comprises 96 patients total, representing 44 unilateral procedures and 52 bilateral procedures (Wells et al., 2022). Transplantation is necessarily a multidisciplinary procedure accompanied by many challenges, including the effects of immunosuppression. However, the procedure can lead to return of sensation, movement, and ability to perform more activities with the hand than with the previous prosthesis, with associated improvement in the patient's quality of life. Transplantation can be successful when initiated as long as 50 years following the initial amputation (Frey et al., 2008; Madden et al., 2019).

Improvements in sensation and mobility for a transplanted hand rely on neuroplasticity, the changes in brain structure and function that occur in response to both experience and injury (Buonomano and Merzenich, 1998; Feldman and Brecht, 2005; Merenstein et al., 2023a; Poldrack, 2000; Taub et al., 2002). Neuroimaging studies with magnetic resonance imaging (MRI) of brain structure have documented loss of gray matter volume and white matter microstructure in brain regions related to amputated limbs (Makin et al., 2013; Simoes et al., 2012). Functional MRI (fMRI) studies suggest that, following amputation, cortical regions representing a missing limb undergo remapping, such that the deafferented cortical region will respond to stimulation at other

* Corresponding author. Duke University Medical Center, Durham, NC, 27710, USA.
E-mail address: david.madden@duke.edu (D.J. Madden).

https://doi.org/10.1016/j.ynirp.2024.100222
Received 27 February 2024; Received in revised form 16 September 2024; Accepted 18 September 2024
Available online 21 September 2024

bodily locations (e.g., face), particularly for individuals with phantom limb pain (Flor et al., 1995; Lotze et al., 2001; but cf. Makin et al., 2015b). Stimulation or movement of the intact hand often leads to fMRI activation of ipsilateral sensorimotor regions (Lotze et al., 2001; Neugroschl et al., 2005; Valyear et al., 2020), as well as to contralateral activation, a pattern that may represent a disruption of normally existing interhemispheric inhibition (Frey et al., 2008; Madden et al., 2019; Philip et al., 2022). In addition, amputation appears to disrupt the functional connectivity of regions within sensorimotor cortex and lead to increased connectivity to other networks, such the default mode network comprising medial prefrontal and parietal regions (Makin et al., 2015a). Despite these changes in cortical organization, the core topography of the sensorimotor network remains stable after amputation (Makin and Bensmaia, 2017).

Following hand transplantation, remapped sensorimotor brain regions contralateral to the transplanted hand return to a more canonical organization, over the initial several months postoperatively. Though inter-individual variability is prominent, the location and amplitude of fMRI activation, both for somatosensory regions responding to sensory stimulation, and for motor regions controlling movement and grasping, gradually become more similar to those exhibited by healthy individuals (Brenneis et al., 2005; Frey et al., 2008; Giraux et al., 2001; Hernandez-Castillo et al., 2016; Madden et al., 2019; Neugroschl et al., 2005; Petruzzo et al., 2006; Philip et al., 2022; Valyear et al., 2019). From fMRI activation associated with visually guided grasping, obtained for a hand transplant patient at 26 and 41 months postoperatively, Valyear et al. proposed that the recovery of sensorimotor function relies on a core network of brain regions including anterior parietal, dorsal and ventral premotor regions, and cerebellum.

In contrast to fMRI activation, Hernandez-Castillo et al. (2018) investigated changes in fMRI connectivity, defined by the correlations among resting-state fMRI signal timeseries for regions of interest, for both a sensorimotor network (defined from a motor cortex seed region) and a default mode network (defined from a posterior cingulate seed region). These authors observed that, for their patient, across four years following bilateral hand transplantation, functional connectivity within the sensorimotor network increased, whereas functional connectivity between the sensorimotor and default mode networks decreased. The Hernandez-Castillo et al. functional connectivity data, as well as the sensorimotor activation findings from other hand transplant studies, are consistent with a more general theme in the brain injury literature, that over the course of recovery, the disrupted brain network gradually begins to resemble what is observed in healthy individuals (Nakamura et al., 2009).

While this pattern of gradual return to a more canonical sensorimotor network is important for understanding the recovery of function following hand transplantation, previous studies are limited in that a preoperative fMRI baseline for the patient is rarely available. Comparison of postoperative data can be conducted with healthy controls, but comparison is complicated by amputation-related cortical reorganization in the hand transplant patient. In the extant literature on hand transplantation, a preoperative fMRI baseline is available for three patients (Giraux et al., 2001; Neugroschl et al., 2005; Petruzzo et al., 2006). All of these are fMRI activation studies; the only study to address changes in brain connectivity following hand transplantation (Hernandez-Castillo et al., 2018) comprised only postoperative assessments. In addition, no previous investigation of hand transplantation has addressed the issue of structural brain connectivity. Recent developments in diffusion-weighted imaging (DWI), in particular, have provided valuable information regarding the strength and organization of white matter fiber tracts (Clayden, 2013; Damoiseaux and Greicius, 2009; Hagmann et al., 2008; Honey et al., 2009; Yeh et al., 2021), which underlie functional brain activation and connectivity.

Here, we report, for the first time, changes in both functional and structural brain connectivity following hand transplantation, with a preoperative baseline. Resting-state fMRI and structural DWI MRI data were acquired for a bilateral hand transplant patient, at approximately four months preoperatively, and then at each of three postoperative visits, separated by approximately six months. The patient's MRI protocol was identical across the testing sessions. It was thus possible to quantify changes in selected measures of the patient's functional and structural brain connectivity, from the preoperative testing session to approximately 1.5 years postoperatively. We also selected data from 10 healthy, community-dwelling adults, age-matched to the patient, with resting-state functional and structural MRI protocols similar to those of the patient (though at a single point in time), to provide a comparison for the patient's data.

As a theoretical context for interpreting these functional and structural data, we used graph theoretical analyses (Bullmore and Sporns, 2009; Rubinov and Sporns, 2010; Sporns, 2011; Sporns and Betzel, 2016), which characterize the brain as a set of modules (or networks), where each module comprises edges of varying strength among anatomically defined nodes. We used a network partition of four modules derived empirically from the patient's preoperative resting-state fMRI data, which provided a common metric for the patient's functional and structural data across all time points, and for the control participants' data. The modules derived in this manner included a sensorimotor module that resembled a corresponding module in a widely used partition of resting-state functional data (Yeo et al., 2011). We focused primarily on two graph theoretical indices: within-module and between-module connectivity strength, for both the functional and structural data, especially for the sensorimotor module. Our overarching hypothesis was that the patient's within- and between-module connectivity, for both the functional and structural measures, would change over the postoperative period to more closely resemble the control participants' values. We also distinguished hand-related from non-hand nodes within the sensorimotor module, with the expectation that the observed changes would be more pronounced for hand-related nodes. Finally, assuming that structural connectivity constraints functional connectivity (Hagmann et al., 2008; Honey et al., 2009), we examined the correlation between the patient's functional and structural measures at each time point.

2. Methods

2.1. Patient and control participants

Surgical and research procedures were conducted at the Duke University Medical Center. This study was conducted in compliance with the Code of Ethics of the World Medical Association (Declaration of Helsinki) for experiments involving humans and with the Duke University Medical Center Institutional Review Board (IRB # 00056079, clinicaltrials.gov # NCT02310867). The patient provided informed consent and received extensive preoperative education and evaluation.

The patient was a right-hand dominant female who was 60 years, 11 months of age at the time of the bilateral hand transplantation (November 2018). The patient had been in normal health until April 2017, when she developed sepsis (group A Streptococcus) with extended intubation, in the intensive care unit, on extracorporeal membrane oxygenation. She required quadri-membral amputations, bilateral below the elbows and above and below the knees.

The patient had completed one year of college, and estimated general intelligence was in the high normal range at the 79th percentile, as estimated from the Wechsler Abbreviated Scale of Intelligence (WASI). To establish a comparison data set for these analyses, we selected 10 individuals from a separate research protocol comprising healthy, community-dwelling adults (Madden et al., 2024; Merenstein et al., 2023b), who were comparable in age to the patient and had the same MRI modalities available. These controls were 55–67 years of age (M = 60.4 years, SD = 4.43; five female), without evidence of cognitive or motor impairment. The mean score on the Mini-Mental State Exam (MMSE; Folstein et al., 1975) for the controls was 29.50 (SD = 0.527).

Brain imaging data for the patient were obtained at a preoperative testing session, approximately four months prior to the hand transplantation (July 2018), and then at each of three postoperative visits, beginning approximately four months after surgery, and then separated by approximately six months (April 2019; November 2019; and June 2020). The control participants' data were obtained in a single testing session. Although the control participants were not followed longitudinally, they were part of a sample of 68 individuals ranging from 18 to 78 years of age (Madden et al., 2024; Merenstein et al., 2023b). Analyses of the imaging data from this larger cohort (Supplementary Material) suggest that relatively little age-related change would be expected over the time period comparable to the patient's preoperative and postoperative testing.

2.2. Transplantation procedure

The donor/recipient pair was matched for blood type, sex, skin color, cytomegalovirus, Epstein-Barr Virus, and limb size. The flow cytometric crossmatch was negative. The procurement of the limbs were performed at the elbow. The transplant procedures were performed simultaneously for both hands following the standard of care for major limb replantation (Meyer, 1991). Briefly, the procedures started with the osteosynthesis of the radius and ulna followed by the vascularization. Flexor and extensor tendon repairs included tendon transfers. Three nerves were repaired in each limb; median, ulnar and superficial branch of the radial nerve. The patient received depletional induction with rabbit antithymocyte globulin (rabbit antithymocyte globulin; Thymoglobulin, Sanofi Genzyme, Cambridge, MA) calculated at 1.5 mg/kg × 3 doses. Maintenance immunosuppression consisted of belatacept 10 mg/kg × 2 doses followed by 5 mg/kg thereafter, as described previously (Cendales et al., 2018). Tacrolimus was dosed to achieve 12-hr trough levels between 10 and 15 ng/mL with conversion to sirolimus at 6 months to achieve trough levels between 8 and 12 ng/mL, mycophenolate mofetil 1 gm BID, and prednisone taper to 10 mg QD. Infectious prophylaxis consisted of fluconazole for three days and valgancyclovir and trimethoprim/sulphamethoxazole for six months. Skin biopsies were taken at predetermined times and at signs of rejection and scored using the Banff scoring system (Cendales et al., 2008). The patient was discharged from the hospital on postoperative day 11 and began occupational therapy on postoperative day 12. The patient returned to our center monthly for belatacept immunosuppression infusion thereafter. At 18 months following the procedure, the patient was able to use both transplanted hands for activities of daily living.

2.3. MRI data acquisition

All imaging data were collected at the Brain Imaging and Analysis Center at Duke University Medical Center on a 3T GE MR750 whole-body MRI scanner (GE Healthcare, Waukesha, WI) equipped with a 60 cm bore and eight-channel receive-only head coil. The imaging parameters were identical for each of the patient's four testing sessions. Each scanning session comprised one T1-weighted image, one run of resting-state T2*-weighted functional images sensitive to the blood oxygen level dependent (BOLD) signal, four runs of event-related T2*-weighted functional images, and one diffusion-weighted image (DWI). The event-related functional data will be reported separately. We focus here on graph theoretical network analyses applied to the resting-state fMRI and DWI structural data.

2.3.1. T1-weighted structural MRI

For the patient, a high-resolution T1-weighted image was acquired using a 3D fast inverse-recovery-prepared spoiled gradient recalled (SPGR) sequence with the following parameters: number of axial slices = 162, repetition time (TR) = 8.21 ms, echo time (TE) = 3.22 ms, inversion recovery time (TI) = 450 ms, field of view (FOV) = 240 mm^2, flip angle = 12^o, voxel size = 1 mm^3, acquisition matrix = 256 mm^2, and a sensitivity encoding (SENSE) factor = 2. For the controls, a high-resolution T1-weighted image was acquired using a 3D fast inverse-recovery-prepared SPGR sequence with the following parameters: number of axial slices = 292, TR = 2203.5 ms, TE = 3.076 ms, TI = 900 ms, FOV = 240 mm^2, flip angle = 8^o, voxel size = 0.47 × 0.47 × 0.5 mm, acquisition matrix = 512 mm^2, and a SENSE factor = 2.

2.3.2. Resting-state fMRI

For the patient, at each testing session, a single T2*-weighted gradient-echo, echo planar imaging (EPI) sequence was acquired during rest (eyes open) with the following parameters: number of slices = 36, TR = 2000 ms, TE = 28 ms, FOV = 240 mm^2, flip angle = 90^o, voxel size = 3.75 × 3.75 × 3.80 mm, acquisition matrix = 64 mm^2, number of volumes = 256, scan time = 8.5 min, and a SENSE factor = 1. For the controls, a single T2*-weighted gradient-echo, EPI sequence was acquired during rest (eyes open) with the following parameters: number of slices = 50, TR = 1500 ms, TE = 30 ms, FOV = 256 mm^2, flip angle = 60^o, voxel size = 2 mm^2, acquisition matrix = 128 mm^2, number of volumes = 300, scan time = 7.5 min, and a SENSE factor = 2.

2.3.3. Diffusion-weighted imaging (DWI)

For the patient, a diffusion-weighted single-shot spin-echo, EPI sequence was acquired with the following parameters: number of axial slices = 72, TR = 10000 ms, TE = 81.8 ms, FOV = 240 mm^2, flip angle = 90^o, voxel size = 2 mm^3, acquisition matrix = 120 mm^2, and a SENSE factor = 2. Diffusion-weighting gradients were applied in 26 directions with a b value of 1000 s/mm^2, with a single non-diffusion-weighted b = 0 image. For the controls, a diffusion-weighted single-shot spin-echo, EPI sequence was acquired with the following parameters: number of axial slices = 92, TR = 4894 ms, TE = 64.7 ms, FOV = 220 mm^2, flip angle = 90^o, voxel size = 1.5 mm^3, acquisition matrix = 144 mm^2, multiband factor = 3, and a SENSE factor = 1. Diffusion-weighting gradients were applied in 90 directions with two b values (1500 or 3000 s/mm^2), with two non-diffusion-weighted b = 0 images. For six of the 10 controls, a second diffusion-weighted scan of six volumes in the reverse phase encoding direction was also obtained with identical parameters, except that TR = 5260 ms, allowing for the subsequent correction of susceptibility-induced distortions.

2.4. MRI data processing

2.4.1. Resting-state fMRI

We preprocessed the resting-state T2*-weighted functional images with fMRIPrep (Esteban et al., 2019) and xcpEngine (https://xcpengine.readthedocs.io/), which implement tools from FSL (FMRIB Software Library; Smith et al., 2004), AFNI (Analysis of Functional NeuroImages; Cox, 1996), and ANTs (Advanced Normalization Tools; Avants et al., 2011). For each of the controls, and at each testing session for the patient, the initial four volumes of the resting-state scan (disabled data acquisitions; disdaqs) were averaged to create a reference image. This reference was then registered to the skull-stripped T1-weighted image using a boundary-based registration cost-function (Greve and Fischl, 2009), allowing the estimation of susceptibility distortions in the absence of fieldmaps (Treiber et al., 2016).

Within fMRIPrep, we estimated head-motion parameters with respect to the fMRI reference image (transformation matrices, and six corresponding rotation and translation parameters), before any spatio-temporal filtering, for subsequent confound regression. Slice timing correction and resampling of the corrected resting-state data were performed in native space by applying a single, composite transform to correct for head motion and susceptibility distortions. Spatial smoothing was not performed, to avoid potential effects on functional network estimation (Alakörkkö et al., 2017).

We then processed the fMRIPrep output with xcpEngine. The first four brain volumes of the resting-state data (disdaqs) were removed to ensure that the steady state equilibrium was attained. For confound

regression, we included the six motion parameters, two physiological regressors (mean white matter [WM] signal and mean cerebral spinal fluid [CSF] signal), the temporal derivatives of these eight regressors, and the quadratic expansions of these eight regressors and of the eight temporal derivatives, yielding 32 nuisance regressors (Satterthwaite et al., 2013). These steps are equivalent to the Model 8 option (36 parameters plus motion scrubbing) described by (Ciric et al., 2017), without the four parameters related to global signal regression. We did not include global signal regression because this processing step can introduce features to the data set (e.g., negative correlations) that are difficult to interpret (Ciric et al., 2017; Murphy and Fox, 2017). Finally, temporal band-pass filtering (0.01 Hz–0.08 Hz) was performed.

Before motion scrubbing, mean framewise displacement (Power et al., 2012) during the resting-state scan was 0.153 mm ($SD = 0.014$) for the patient and 0.135 mm ($SD = 0.071$) for the controls, and these values did not significantly differ, $p = 0.632$. Before construction of resting-state functional connectivity correlation matrices (see the later section, *Functional and Structural Connectivity Estimation*), we performed motion scrubbing of resting-state volumes with >0.50 mm using spectral interpolation. If fewer than five volumes remained between two outlier volumes, both outliers and all the intervening volumes were scrubbed to account for residual motion (Ciric et al., 2017; Parkes et al., 2018; Power et al., 2014). For the patient, no more than 2% of volumes were scrubbed from an individual testing session. For the controls, motion scrubbing was only necessary for one participant (14% of volumes). Following motion scrubbing, the residualized image from xcpEngine data was registered to a standard Montreal Neurological Institute (MNI) template (2 mm^3 resolution) using *antsRegistration*.

2.4.2. Diffusion-weighted imaging (DWI)

We preprocessed the DWI data using MRtrix3 (http://mrtrix.org; Tournier et al., 2019), which also implements tools from FSL and ANTs. The DWI data were first denoised and then corrected for head motion and eddy current-induced distortions (Bastiani et al., 2019). For six of the control participants, DWI data were acquired in opposing directions, and susceptibility-induced distortions were corrected by applying FSL's *topup*. Lastly, all data were bias-corrected using the *dwibiascorrect* command in MRtrix. All DWI data were visually inspected and found to be acceptable for brain mask coverage, quality of motion and susceptibility-induced distortion correction, MR artifacts (e.g., ghosting, RF inhomogeneities) and anatomical abnormalities.

From these preprocessed images, Fiber Orientation Distribution (FOD) maps were then derived using multi-shell multi-tissue constrained spherical deconvolution (Tournier et al., 2019), based on tissue-specific response functions from three compartments (gray matter, [GM], WM, and CSF) from the controls' multi-shell DWI data and two compartments (WM and CSF) from the patient's single-shell DWI data. From the FOD maps, we generated streamlines using anatomically constrained probabilistic tractography (ACT; Smith et al., 2012), which limits the extent of streamline propagation and ensures proper termination of streamlines in the GM/WM interface. We set the maximum streamline length to 250 mm and the FOD amplitude cutoff to 0.06. For each control participant and each testing session for the patient, 10 million tracts were generated and iteratively filtered by a factor of 10 to 1 million streamlines via spherical-deconvolution informed filtering of tractograms (*tcksift*) in MRtrix (Smith et al., 2013). SIFT identifies false positive tracts that do not match the underlying white-matter anatomy via minimization of a cost-function based on the FOD (Ye et al., 2016). The filtered streamlines were then transformed to the same 2 mm^3 MNI152 template as the resting-state data.

2.5. Functional and structural connectivity estimation

Graph theoretical analyses (Bullmore and Sporns, 2009; Rubinov and Sporns, 2010; Sporns, 2011; Sporns and Betzel, 2016) are based on a set of anatomically defined set of regions (nodes). We used the nodes defined by the Brainnetome Atlas (Fan et al., 2016), which comprises 274 brain regions derived from probabilistic tractography using *in vivo* DWI data. Our MRI slice prescription for the T2*-weighted functional images did not fully cover the cerebellum for either the patient or controls, and thus we eliminated the 28 cerebellar nodes. Similarly, the functional images included fewer than 50% of voxels in five inferior temporal nodes for both the patients and controls, and these five nodes were also eliminated. This final set of 241 nodes was used in all subsequent analyses of the fMRI and DWI data.

For the resting-state fMRI data, we used a beta timeseries approach to construct a 241 × 241 matrix of pairwise correlation coefficients (Pearson *r*) among the nodes, separately for each control participant and each testing session for the patient. Because there is ambiguity regarding the interpretation of negative correlations, these were set to zero, as recommended by (Rubinov and Sporns, 2010). The matrix diagonal was excluded from the calculations. The final matrix cells were the pairwise correlations (Fisher *r*-to-*z* transformed) for the timeseries at each node. We conducted analyses on undirected, weighted matrices, rather than on thresholded matrices, to retain sensitivity to this variation in connection strength (Rubinov and Sporns, 2011).

From the DWI data, the endpoint of each streamline was assigned to the nearest gray matter node using the default 4 mm radial search option (Smith et al., 2015). We then constructed a symmetrical, weighted matrix of 241 × 241 cells representing the total number of filtered streamlines connecting each pair of nodes, scaled to account for differences in node volume (Hagmann et al., 2008). Although the T1-weighted MRI data are also structural data, these images were used only for registration. Here, the term structural connectivity refers to the connectivity strength (number of streamlines) between nodes, estimated from the DWI data.

2.6. Modules of functional connectivity

Modules are defined from sets of nodes that are more highly connected to each other than to other nodes. Several partitions of resting-state fMRI data are available (Gordon et al., 2014; Ji et al., 2019; Power et al., 2011; Yeo et al., 2011), which would provide an independent definition of modular structure. These partitions, however, are based primarily on data from younger adults, whereas the patient was nearly 61 years of age at the preoperative time point. More critically, it is likely that the amputations that the patient had undergone in the year prior to the preoperative testing would have led to some degree of functional and structural reorganization of brain networks (Bramati et al., 2019; Flor et al., 1995; Makin et al., 2015a), further decreasing the validity of an independently applied network partition. To define the modules relevant for analyses of connectivity, we therefore used the data from the patient's first (preoperative) testing session. We conducted a modularity analysis of the preoperative resting-state fMRI data using the Brain Connectivity Toolbox (Rubinov and Sporns, 2010) and then applied the modules defined at this preoperative session to data at the postoperative testing sessions, and to the control participants' data. This approach provides a common metric for the change in the patient's functional connectivity over time, and for the comparison to the control participants. We also applied the modules defined from the preoperative resting-state fMRI data to the DWI data. Thus, when interpreting the differences in the graph theoretical measures in connectivity, both over time and in relation to the control participants, it is important to note that these differences refer specifically to this patient's preoperative modular structure and may not generalize beyond it. Similarly, these modules, being defined from functional data, would not be expected to correspond to structural modules derived from DWI data. Our goal with the DWI data, however, was not to define structural modules, but rather to estimate the strength of structural connectivity, and change over time, within the modules derived from the preoperative, functional data.

Using the 241 × 241 correlation matrices for the patient's resting-state fMRI data at the preoperative session, we determined the

assignment of nodes to modules using 150 iterations of the Louvain algorithm (Blondel et al., 2008), with the default setting (1.0) of the spatial resolution parameter (gamma). Next, we calculated the average agreement matrix across these 150 iterations, retaining values for only those pairs of nodes that were assigned to the same module for at least 50% of the iterations, and applied consensus clustering (Lancichinetti and Fortunato, 2012) to obtain the final consensus modules. This partition identified four modules in the patient's preoperative resting-state fMRI data. The present analyses focused on one of these modules, comprising 43 nodes, consistent with a sensorimotor network (SMN), centered on the pre- and post-central gyri and subcortical regions (Fig. 1). Of these nodes, 21% ($n = 9$) were subcortical regions, and 59% ($n = 20$) of the remaining 34 nodes aligned with a standard partition of a SMN in healthy younger adults (Yeo et al., 2011). Individual nodes on the precentral and postcentral gyri are illustrated in Supplementary Fig. 1. Additional analyses applying the Yeo seven-module partition to the present data yielded differences in the pattern of connectivity (Supplementary Material), and we thus emphasize that the present findings are specific to this method, in which we use the modular partition from the patient's preoperative data as the metric of comparison.

To determine whether any changes in connectivity were specific to hand-related nodes in the SMN, we further classified each node within this module as either hand-related or not (Fig. 1), based on the functional description for each node, within the Brainnetome graphical user interface (https://atlas.brainnetome.org/bnatlas.html). The functional descriptions are behavioral domain and paradigm class meta data labels following the BrainMap taxonomy (http://www.brainmap.org/taxonomy). A node was classified as hand-related if the paradigm class descriptor included the terms any of the following terms: writing, grasping, drawing, pointing, or finger-tapping. Fifteen nodes met these criteria. Two additional nodes were associated with finger tapping but were located in the precentral and postcentral gyri of the left hemisphere, in regions associated anatomically the tongue and larynx, and these two nodes were considered to be non-hand related, yielding 28 nodes for the non-hand module. The assignment of nodes to the hand-related and non-hand modules, within the SMN, is presented in Supplementary Table 1. Analyses deleting the two reassigned nodes indicated that they did not substantially influence the pattern of results (Supplementary Table 2).

For each testing session for the patient, and for each control participant, we then calculated within-module and between-module connectivity for each node, comparing the average of the nodes within the SMN to the average of the nodes within the three non-SMN modules, and also when considering the hand-related and non-hand nodes as separate modules within the SMN. With the relatively limited sample of 43 anatomical nodes within the SMN module, which were distributed over left and right cerebral hemispheres, we did not attempt to identify hemisphere-specific patterns of connectivity.

3. Results

3.1. Statistical analyses

Analysis of variance (ANOVA) and regression were conducted using SAS 9.4 (SAS Institute, Inc., Cary, NC, USA), within the general linear model. The control participants' data for each node were first averaged across participants, so that the data sets for the patient and controls were comparable, each with values for 241 nodes. We first compared the patient and control participants' data (both resting-state fMRI and DWI structural data) at the preoperative testing session, using group (patient vs. controls) and module (SMN vs. non-SMN; hand-related vs. non-hand), as fixed effects, and node (nested within module) as a random effect, in the estimation of the variance components. We then tested the patient's data separately, using module and testing session (preoperative and three postoperative) as fixed effects and node (nested within module) as a random effect. Note that estimates of within-module connectivity are specific to individual modules, whereas in analyses comparing two modules (i.e., SMN vs. non-SMN nodes; Hand vs. non-Hand), between-module connectivity is by definition identical for the two modules. To follow up significant effects of testing session, we used Dunnett's *t*-test for comparisons with a control mean (Dunnett, 1955), comparing each of the patient's sessions to the data from the control participants, Bonferroni corrected for multiple comparisons (i.e., alpha

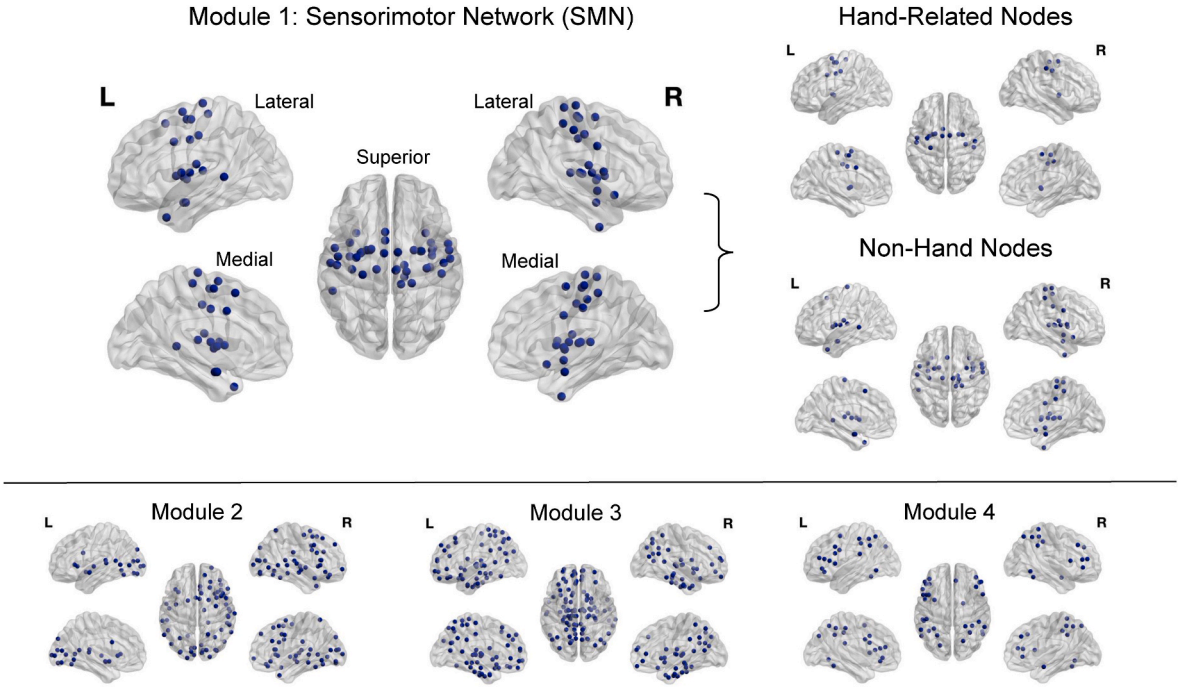

Fig. 1. Module partition. Four data-driven modules were derived from the patient's preoperative resting-state fMRI data, using Brainnetome Atlas nodes (Fan et al., 2016) and the Brain Connectivity Toolbox (Rubinov and Sporns, 2010), with the Louvain algorithm and consensus clustering.

= 0.0125).

3.2. Resting-state functional connectivity

3.2.1. Sensorimotor network (SMN) vs. non-SMN modules: within-module connectivity

At the preoperative testing session, comparing the SMN and non-SMN modules, within-module functional connectivity was higher for the patient than for the controls, F (1, 239) = 238.71, $p < 0.0001$, but neither the main effect of module nor the Group × Module interaction was significant (Fig. 2A).

In the patient's within-module connectivity data, the effect of session was significant, F (3, 717) = 71.89, $p < 0.0001$, reflecting a decrease in connectivity over time (Fig. 2A). The main effect of module was not significant, but the Module × Session interaction was significant, F (3, 717) = 5.37, $p < 0.01$, because connectivity for the SMN decreased consistently across sessions, whereas the non-SMN connectivity showed a decrease from the preoperative session to the second postoperative session, and then an increase between the second and third postoperative sessions. However, the difference between the patient's SMN and non-SMN within-module connectivity was not significant at any testing session considered individually. For both the SMN and non-SMN nodes, the patient's within-module functional connectivity was significantly higher than that of the controls, at each testing session (Table 1).

3.2.2. Sensorimotor network (SMN) vs. Non-SMN modules: between-module connectivity

Because the SMN and non-SMN comparison comprises only two modules, the between-module connectivity values (Fig. 2B) are the same for each module. In the patient's data, the effect of testing session was significant for between-module connectivity, F (3, 126) = 8.13, $p < 0.0001$, although the connectivity did not exhibit a consistent change over time (Fig. 2B). The patient's connectivity was higher than that of the controls at the preoperative testing session and at the second postoperative session (Table 2).

3.2.3. Hand-related vs. non-hand nodes within the sensorimotor network (SMN): within-module connectivity

Within the SMN, at the preoperative testing session, with the patient and control data combined, hand-related nodes exhibited higher within-module functional connectivity relative to non-hand nodes, F (1, 41) = 48.56, $p < 0.0001$ (Fig. 3A). In addition, connectivity was higher for the patient than for the controls, F (1, 41) = 395.16, $p < 0.0001$, and the Group × Module interaction was significant, F (1, 41) = 19.76, $p < 0.0001$. This interaction reflects the fact that the increased connectivity for hand nodes relative to non-hand nodes was greater in magnitude for the patient than for the controls, though significant in each case, with F (1, 41) > 29.0, $p < 0.0001$.

For the patient's data, the effect of session was significant, F (3, 123) = 83.38, $p < 0.0001$, with a consistent decrease in within-module connectivity over time, and connectivity was higher for hand-related nodes than for non-hand nodes, F (1, 41) = 43.87, $p < 0.0001$ (Fig. 3A). The Module × Session interaction was also significant, F (3,

Table 1
Comparison between the patient and controls, for functional within-module connectivity of sensorimotor network (SMN) nodes and non-SMN nodes, at each testing session.

Comparison	Difference	Lower CI	Upper CI
	SMN Nodes		
Pre-Op vs. Controls	0.2357	**0.1992**	**0.2722**
Post-Op Session 1 vs. Controls	0.1296	**0.0932**	**0.1661**
Post-Op Session 2 vs. Controls	0.0926	**0.0561**	**0.1291**
Post-Op Session 3 vs. Controls	0.0443	**0.0078**	**0.0808**
	Non-SMN Nodes		
Pre-Op vs. Controls	0.2017	**0.1729**	**0.2304**
Post-Op Session 1 vs. Controls	0.1108	**0.0820**	**0.1395**
Post-Op Session 2 vs. Controls	0.0706	**0.0418**	**0.0993**
Post-Op Session 3 vs. Controls	0.0924	**0.0637**	**0.1212**

Note. n = 43 SMN nodes and 198 non-SMN nodes. Pre-Op = Preoperative; Post-Op = Postoperative; Difference = Difference between mean values. Upper/Lower CI = 98.75% confidence intervals for the significance of the Dunnett's t-test for comparisons to a control mean, with alpha = 0.0125. Significant comparisons (i.e., CIs that do not include zero) have the Upper/Lower CI values in bold.

Table 2
Comparison between the patient and controls, for functional between-module connectivity of sensorimotor network (SMN) nodes and non-SMN nodes, at each testing session.

Comparison	Difference	Lower CI	Upper CI
Pre-Op vs. Controls	0.0491	**0.0266**	**0.0715**
Post-Op Session 1 vs. Controls	0.0185	−0.0040	0.0409
Post-Op Session 2 vs. Controls	0.0301	**0.0077**	**0.0526**
Post-Op Session 3 vs. Controls	0.0116	−0.0109	0.0340

Note. n = 43 SMN nodes and 198 non-SMN nodes. Pre-Op = Preoperative; Post-Op = Postoperative; Difference = Difference between mean values. Upper/Lower CI = 98.75% confidence intervals for the significance of the Dunnett's t-test for comparisons to a control mean, with alpha = 0.0125. Significant comparisons (i.e., CIs that do not include zero) have the Upper/Lower CI values in bold.

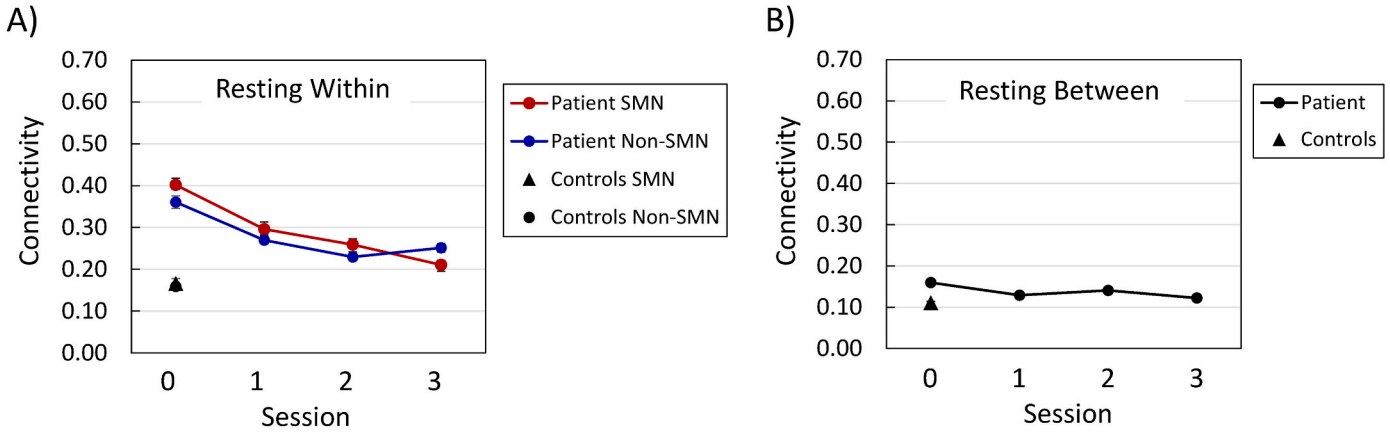

Fig. 2. Resting-state functional connectivity of sensorimotor network (SMN) nodes and non-SMN nodes, at each testing session. Panel A = within-module connectivity; Panel B = between-module connectivity. Session 0 was approximately four months preoperative, and each subsequent session occurred at approximately six-month intervals (see *Patient and Control Participants*).

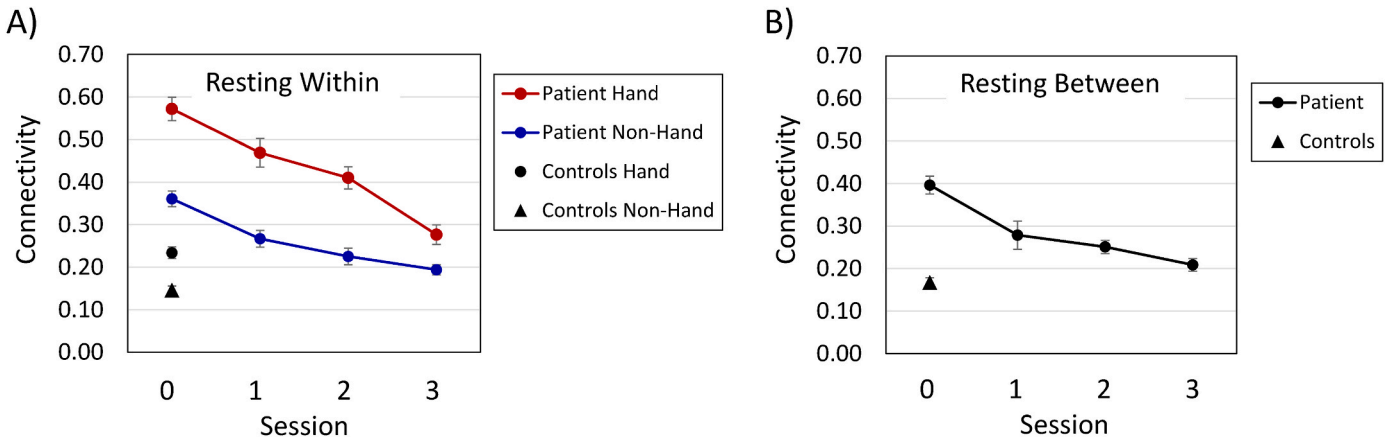

Fig. 3. Resting-state functional connectivity of hand and non-hand nodes within the sensorimotor network, at each testing session. Panel A = within-module connectivity; Panel B = between-module connectivity. $n = 15$ hand nodes and 28 non-hand nodes. Session 0 was approximately four months preoperative, and each subsequent session occurred at approximately six-month intervals (see *Patient and Control Participants*).

123) = 7.90, $p < 0.0001$, because the higher connectivity for hand-related nodes, relative to non-hand nodes, was greater preoperatively than postoperatively, but the decrease in connectivity over time was significant for both modules, with $F > 39.0$, $p < 0.0001$, in each case (Table 3). For hand-related nodes, within-module connectivity was higher for the patient than for the controls at the preoperative session, and at postoperative sessions 1 and 2, but at postoperative session 3 within-module connectivity for these nodes was comparable for the patient and the controls. In contrast, the patient's within-module connectivity for non-hand nodes decreased over time but remained significantly higher than that of the controls at each testing session.

3.2.4. *Hand-related vs. non-hand nodes within the sensorimotor network (SMN): between-module connectivity*

For the patient's data, the between-module connectivity for the hand-related and non-hand nodes decreased over time, F (3, 42) = 19.24, $p < 0.0001$ (Fig. 3B). Connectivity was significantly higher for the patient than for controls at the preoperative and first two postoperative sessions, and then connectivity values were comparable for the patient and controls at the third postoperative session (Table 4).

Table 3
Comparison between the Patient and controls, for functional within-module connectivity of hand-related and non-hand nodes, within the sensorimotor network (SMN), at each testing session.

Comparison	Difference	Lower CI	Upper CI
Hand-Related Nodes			
Pre-Op vs. Controls	0.3382	**0.2601**	**0.4164**
Post-Op Session 1 vs. Controls	0.2352	**0.1571**	**0.3133**
Post-Op Session 2 vs. Controls	0.1766	**0.0985**	**0.2547**
Post-Op Session 3 vs. Controls	0.0427	−0.0355	0.1208
Non-Hand Nodes			
Pre-Op vs. Controls	0.2145	**0.1695**	**0.2595**
Post-Op Session 1 vs. Controls	0.1206	**0.0756**	**0.1656**
Post-Op Session 2 vs. Controls	0.0790	**0.0340**	**0.1240**
Post-Op Session 3 vs. Controls	0.0477	**0.0027**	**0.0927**

Note. $n = 15$ Hand-related nodes and 28 non-Hand nodes. Pre-Op = Preoperative; Post-Op = Postoperative; Difference = Difference between mean values. Upper/Lower CI = 98.75% confidence intervals for the significance of the Dunnett's t-test for comparisons to a control mean, with alpha = 0.0125. Significant comparisons (i.e., CIs that do not include zero) have the Upper/Lower CI values in bold.

Table 4
Comparison between the patient and controls, for functional between-module connectivity of hand-related and non-hand nodes, within the sensorimotor network (SMN), at each testing session.

Comparison	Difference	Lower CI	Upper CI
Pre-Op vs. Controls	0.2291	**0.1542**	**0.3039**
Post-Op Session 1 vs. Controls	0.1114	**0.0366**	**0.1862**
Post-Op Session 2 vs. Controls	0.0839	**0.0091**	**0.1587**
Post-Op Session 3 vs. Controls	0.0415	−0.0333	0.1164

Note. $n = 15$ Hand-related nodes and 28 Non-hand nodes. Pre-Op = Preoperative; Post-Op = Postoperative; Difference = Difference between mean values. Upper/Lower CI = 98.75% confidence intervals for the significance of the Dunnett's t-test for comparisons to a control mean, with alpha = 0.0125. Significant comparisons (i.e., CIs that do not include zero) have the Upper/Lower CI values in bold.

3.3. *Diffusion-weighted imaging (DWI) structural connectivity*

3.3.1. *Sensorimotor network (SMN) vs. Non-SMN modules: within-module connectivity*

Analyses of the within-module, structural connectivity, for the functionally defined SMN and non-SMN modules, at the preoperative testing session, yielded significant effects for the patient vs. controls, F (1, 239) = 40.35, $p < 0.0001$, module, F (1, 239) = 22.33, $p < 0.0001$, and the Group × Module interaction, F (1, 239) = 22.84, $p < 0.0001$ (Fig. 4A). These findings represent a pattern in which connectivity was higher for SMN nodes than for non-SMN nodes for the patient, F (1, 239) = 24.49, $p < 0.0001$, but not for the controls, F (1, 239) < 1.0. In Fig. 4A, the data points for the patient's non-SMN nodes at the preoperative testing session, and the controls' SMN and non-SMN nodes, all overlap. The relatively higher within-module structural connectivity for SMN nodes was also evident in the patient's session data, F (1, 239) = 24.16, $p < 0.0001$ (Fig. 4A). The effects of testing session, F (3, 717) = 3.0, $p < 0.05$, and the Module × Session interaction, F (3, 717) = 3.20, $p < 0.05$, were also significant, but these effects represent relatively minor fluctuations in the connectivity values. The session effect was not significant for either the SMN or non-SMN modules considered individually. The connectivity values were higher for the patient than for the controls at all testing sessions for the SMN nodes, but at none of the testing sessions for the non-SMN nodes (Table 5).

3.3.2. *Sensorimotor network (SMN) vs. Non-SMN modules: between-module connectivity*

In the patient's data, the effect of testing session was not significant for between-module structural connectivity, F (3, 126) < 1.0 (Fig. 4B),

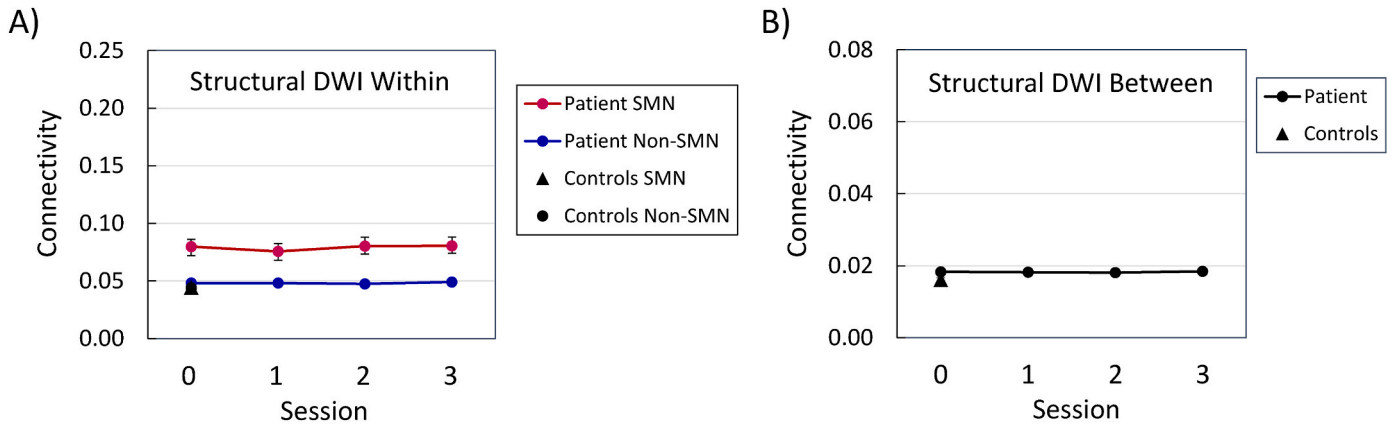

Fig. 4. Diffusion-weighted imaging (DWI) structural connectivity of sensorimotor network (SMN) nodes and non-SMN nodes, at each testing session. Panel A = within-module connectivity; Panel B = between-module connectivity. Session 0 was approximately four months preoperative, and each subsequent session occurred at approximately six-month intervals (see *Patient and Control Participants*).

Table 5
Comparison between the patient and controls, for structural within-module connectivity of sensorimotor network (SMN) nodes and non-SMN nodes, at each testing session.

Comparison	Difference	Lower CI	Upper CI
	SMN Nodes		
Pre-Op vs. Controls	0.0354	**0.0209**	**0.0499**
Post-Op Session 1 vs. Controls	0.0313	**0.0168**	**0.0458**
Post-Op Session 2 vs. Controls	0.0359	**0.0214**	**0.0504**
Post-Op Session 3 vs. Controls	0.0361	**0.0216**	**0.0506**
	Non-SMN Nodes		
Pre-Op vs. Controls	0.0050	−0.0001	0.0101
Post-Op Session 1 vs. Controls	0.0041	−0.0001	0.0092
Post-Op Session 2 vs. Controls	0.0041	−0.0001	0.0092
Post-Op Session 3 vs. Controls	0.0034	−0.0017	0.0085

Note. n = 43 SMN nodes and 198 non-SMN nodes. Pre-Op = Preoperative; Post-Op = Postoperative; Difference = Difference between mean values. Upper/Lower CI = 98.75% confidence intervals for the significance of the Dunnett's t-test for comparisons to a control mean, with alpha = 0.0125. Significant comparisons (i.e., CIs that do not include zero) have the Upper/Lower CI values in bold.

and the difference between the patient and controls was not significant at any testing session (Table 6).

3.3.3. *Hand-related vs. non-hand nodes within the sensorimotor network (SMN): within-module connectivity*

Within the SMN, at the preoperative testing session, structural within-module connectivity was higher for hand-related nodes than for non-hand nodes, F (1, 41) = 23.01, $p < 0.0001$ (Fig. 5A). However, neither the difference between the patient and the controls nor the Group × Module interaction was significant. In the patient's data across the testing sessions, the relatively higher connectivity for hand-related nodes was significant, F (1, 41) = 16.89, $p < 0.001$ (Fig. 5A), but neither the main effect of session nor the Module × Session interaction was significant. The difference in connectivity between the patient and controls was not significant at any of the testing sessions, for either the hand-related or non-hand nodes (Table 7).

Table 6
Comparison between the patient and controls, for structural between-module connectivity of sensorimotor network (SMN) nodes and non-SMN nodes, at each testing session.

Comparison	Difference	Lower CI	Upper CI
Pre-Op vs. Controls	0.0023	−0.0007	0.0054
Post-Op Session 1 vs. Controls	0.0020	−0.0011	0.0051
Post-Op Session 2 vs. Controls	0.0021	−0.0001	0.0052
Post-Op Session 3 vs. Controls	0.0022	−0.0001	0.0053

Note. n = 43 SMN nodes and 198 non-SMN nodes. Pre-Op = Preoperative; Post-Op = Postoperative; Difference = Difference between mean values. Upper/Lower CI = 98.75% confidence intervals for the significance of the Dunnett's t-test for comparisons to a control mean, with alpha = 0.0125. None of the comparisons was significant (i.e., CIs that do not include zero).

3.3.4. *Hand-related vs. non-hand nodes within the sensorimotor network (SMN): between-module connectivity*

The patient's structural between-module connectivity, for hand-related and non-hand nodes, did not vary significantly across the testing sessions, F (3, 42) < 1.0 (Fig. 5B), and the comparison between the patient and the controls was not significant at any testing session (Table 8).

3.3.5. *Correlations between functional and structural connectivity*

We calculated the correlation between functional and structural connectivity, for the patient and controls, for within-module and between-module connectivity, across the nodes within the SMN and non-SMN modules, at each testing session (Table 9 and Supplementary Figs. 2–5). Differences between the correlations (Fisher r-to-z transformed), for within-module and between-module connectivity, were tested via a z-test for correlations (Hinkle et al., 1988). For the patient, the correlation between functional and structural connectivity was significantly higher for within-module than for between-module data, for both SMN and non-SMN modules, at each testing session. For the controls, the difference between within-module and between-module correlations was not significant for either the SMN or non-SMN modules.

4. Discussion

These findings represent the first investigation combining functional and structural brain connectivity, with a preoperative baseline, for a hand transplant patient. Across three postoperative time points, spanning approximately 1.5 years, we observed significant changes in graph theoretical measures of brain connectivity. We focused on nodes associated with a SMN module, assuming that this module should be critical for postoperative recovery. This SMN module, defined empirically from the patient's preoperative, resting-state fMRI data (Fig. 1), exhibited some resemblance to a widely used network partition based on healthy younger adult data (Yeo et al., 2011), demonstrating an underlying preservation of sensorimotor organization (Makin and Bensmaia, 2017).

The functional connectivity data partially confirm our initial hypothesis that both the within- and between-module connectivity would exhibit postoperative change, in the form of a return to a more canonical organization (Giraux et al., 2001; Hernandez-Castillo et al., 2016; Makin

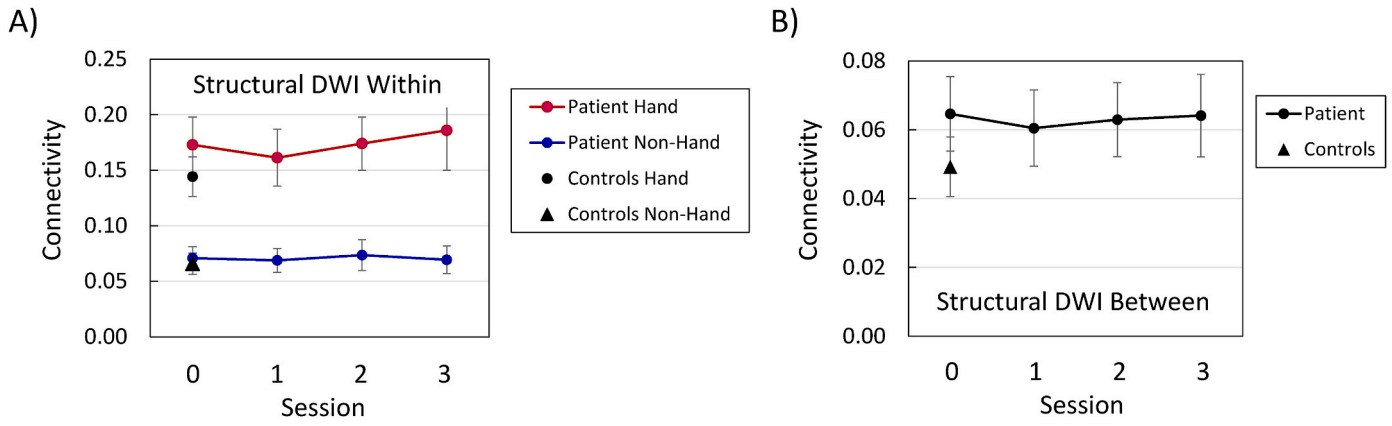

Fig. 5. Diffusion-weighted imaging (DWI) structural connectivity of hand and non-hand nodes within the sensorimotor network, at each testing session. Panel A = within-module connectivity; Panel B = between-module connectivity. n = 15 hand nodes and 28 non-hand nodes. Session 0 was approximately four months pre-operative, and each subsequent session occurred at approximately six-month intervals (see *Patient and Control Participants*).

Table 7
Comparison between the patient and controls, for structural within-module connectivity of hand-related and non-hand nodes, within the sensorimotor network (SMN), at each testing session.

Comparison	Difference	Lower CI	Upper CI
Hand-Related Nodes			
Pre-Op vs. Controls	0.0286	−0.0333	0.0904
Post-Op Session 1 vs. Controls	0.0171	−0.0448	0.0789
Post-Op Session 2 vs. Controls	0.0297	−0.0321	0.0916
Post-Op Session 3 vs. Controls	0.0417	−0.0202	0.1035
Non-Hand Nodes			
Pre-Op vs. Controls	0.0050	−0.0155	0.0254
Post-Op Session 1 vs. Controls	0.0029	−0.0175	0.0234
Post-Op Session 2 vs. Controls	0.0077	−0.0128	0.0281
Post-Op Session 3 vs. Controls	0.0035	−0.0167	0.0239

Note. n = 15 Hand-related nodes and 28 non-Hand nodes. Pre-Op = Preoperative; Post-Op = Postoperative; Difference = Difference between mean values. Upper/Lower CI = 98.75% confidence intervals for the significance of the Dunnett's *t*-test for comparisons to a control mean, with alpha = 0.0125. None of the comparisons was significant (i.e., CIs that do not include zero).

Table 8
Comparison between the patient and controls, for structural between-module connectivity of hand-related and non-hand nodes, within the sensorimotor network (SMN), at each testing session.

Comparison	Difference	Lower CI	Upper CI
Pre-Op vs. Controls	0.0154	−0.0050	0.0359
Post-Op Session 1 vs. Controls	0.0113	−0.0092	0.0317
Post-Op Session 2 vs. Controls	0.0137	−0.0067	0.0342
Post-Op Session 3 vs. Controls	0.0149	−0.0055	0.0354

Note. n = 15 Hand-related nodes and 28 non-Hand nodes. Pre-Op = Preoperative; Post-Op = Postoperative; Difference = Difference between mean values. Upper/Lower CI = 98.75% confidence intervals for the significance of the Dunnett's *t*-test for comparisons to a control mean, with alpha = 0.0125. None of the comparisons was significant (i.e., CIs that do not include zero).

and Bensmaia, 2017; Nakamura et al., 2009; Philip et al., 2022; Valyear et al., 2019). The within-module connectivity data (Fig. 2A) were consistent with this hypothesis. The within-module connectivity, which was higher than that of the controls at the preoperative baseline, decreased consistently across the testing sessions towards the control participants' level. Even at the third session, however, approximately 1.5 years postoperatively, within-module connectivity was higher for the patient than for the controls. Between-module connectivity, in contrast, was relatively constant across the testing sessions, though higher for the patient than for the controls at the preoperative and second postoperative sessions (Fig. 2B). This pattern of initially higher within-module functional connectivity, with a decrease postoperatively towards normal control values, was more pronounced for hand-related nodes within the SMN, relative to non-hand nodes (Fig. 3).

Table 9
Correlations between resting-state fMRI and DWI structural connectivity, as a function of within-module vs. between-module connectivity, module, and testing session, for the patient and control participants' data.

	Within	Between	Difference
	Patient		
SMN			
Pre-op	0.5575***	0.1789	2.005**
Post-Op Session 1	0.4891***	−0.1229	2.945**
Post-Op Session 2	0.5378***	−0.1548	3.386**
Post-Op Session 3	0.6548***	0.0023	3.494**
Non-SMN			
Pre-op	0.4897***	0.1236	4.063**
Post-Op Session 1	0.4530***	0.2490**	2.312*
Post-Op Session 2	0.4716***	0.1707*	3.355**
Post-Op Session 3	0.4247***	0.2132**	0.339*
	Controls		
SMN	0.0887	−0.1430	1.024
Non-SMN	−0.0302	0.0290	−0.264

Note. n = 43 SMN nodes and 198 non-SMN nodes. SMN = Sensorimotor network; Pre-Op = Preoperative; Post-Op = Postoperative. Within = Pearson *r* correlation for resting-state functional and DWI structural within-module connectivity; Between = Pearson *r* correlation for resting-state functional and DWI structural between-module connectivity. Difference = difference between correlations by the Fisher *z*-statistic (*FDR* Corrected).
*$p_{FDR} < 0.05$.
**$p_{FDR} < 0.01$.
***$p_{FDR} < 0.001$.

At the preoperative baseline, the relatively higher within-module functional connectivity for the patient was surprising, in view of a previous report indicating that amputation leads to relatively weakened functional connectivity within the SMN and to increased connectivity between the SMN and other networks, such as the default mode network (Makin et al., 2015a). In addition, Hernandez-Castillo et al. (2018) found that functional connectivity within the SMN, following bilateral hand transplantation, exhibited a pattern different from that observed here, with relatively lower values at an initial assessment (four months postoperative), increasing gradually towards normal control values over the course of four years. Hernandez-Castillo et al. also found that functional connectivity changes were specific to the SMN, with the default mode network connectivity remaining constant postoperatively, whereas our findings suggest a whole-brain change in within-module functional connectivity (Fig. 2A).

The reason for these different patterns of functional connectivity is not clear. Although decreased functional connectivity following amputation has been demonstrated (Hernandez-Castillo et al., 2018; Makin et al., 2015a), Philip et al. (2022) emphasize the wide range of cortical responses that occur in response to amputation. The present findings raise the possibility that increased functional connectivity within modules be also one aspect of amputation-related neural plasticity, expressed as the difference between the patient and controls at the preoperative baseline. In addition, our method for defining functional and structural connectivity, in the context of graph theory, differs from previous measures of fMRI activation and connectivity. We emphasize here the consistent pattern in our patient's data, in the context of our measures, rather than the differences from previous reports. The decline in the patient's within-module functional connectivity, for both SMN and non-SMN modules, across the 1.5 year postoperative interval, towards the values for healthy controls, is consistent with our overarching hypothesis of a return to a more canonical form of brain organization.

In contrast to the functional connectivity data, the patient's structural connectivity data, both within and between modules, did not exhibit a consistent change over time (Fig. 4). However, the patient's within-SMN structural connectivity was significantly higher than that for the control participants (Fig. 4A), suggesting a specific increase in within-SMN structural connectivity, in response to amputation, that had not decreased by 1.5 years following transplantation. Both the patient and controls exhibited higher structural connectivity among hand-related nodes relative to non-hand nodes, and this pattern did not change over the postoperative testing sessions (Fig. 5). Neuroplasticity-related changes in brain function, however, may be detectable earlier than corresponding changes in brain structure (Merenstein et al., 2023a).

Although the patient's functional and structural connectivity data differed, in terms of the degree of change over the postoperative period, the two forms of connectivity were related to each other at each testing session (Table 9). The patient's functional and structural within-module connectivity values, for both SMN and non-SMN modules, were correlated at each of the testing sessions. The between-module connectivity values were correlated only for the non-SMN modules, at the postoperative sessions. The control participants, in contrast, did not exhibit any correlation between functional and structural connectivity. The patient's structural-functional correlations were significantly higher for within-module connectivity as compared to between-module connectivity preoperatively, as well as postoperatively, suggesting that the shared variance among these measures was a response to amputation. Although the correlations alone do not reveal exactly how these functional and structural properties of the brain are interacting, the increased correlations for the patient's within-module values are consistent an enhanced reliance of functional connectivity on structural network organization (Hagmann et al., 2008; Honey et al., 2009).

4.1. Limitations

This first exploration of brain connectivity following hand transplantation, in the context of graph theory, limited the analyses to within- and between-module connectivity. Graph theory provides many other variables characterizing network organization (Bullmore and Sporns, 2009; Rubinov and Sporns, 2010; Sporns, 2011; Sporns and Betzel, 2016), such as the degree to which individual modules are distinct from each other (system segregation) and the strength of an individual node's connections to nodes outside its module (participation coefficient). In addition, graph theoretical measures can vary as a function of the network partition and features of the initial data processing pipeline (Alakörkkö et al., 2017; Fornito et al., 2010; Gargouri et al., 2018; Li et al., 2024; Luppi et al., 2024). We derived a network partition empirically, from the patient's preoperative, resting-state fMRI data, and the results may not generalize beyond this patient's modular structure.

The control participants' data were available from only a single testing session; ideally, we would like to have additional time points to match those of the patient. Analyses of the cross-sectional age-related effects in the larger cohort, from which the control participants were drawn (Supplementary Material) suggest that relatively little change in the imaging measures would be expected, for healthy individuals, over 1.5–2 years. It is also important to note that recovery of function and the underlying neural reorganization are likely to continue beyond the 1.5 year postoperative period reported here (Hernandez-Castillo et al., 2018; Valyear et al., 2019).

Both the patient and control participants' MRI data were acquired at the Duke University Medical Center. Importantly, the scanner hardware and imaging parameters for the patient and controls were constant across the preoperative and postoperative testing sessions. The parameters of the imaging pulse sequences varied slightly between the patient and controls, but the MRI data processing pipeline creating the graph theoretical variables, for both the functional and structural MRI data, was identical for the patient and controls. We also note that for some of our MRI outcome variables, such as functional between-module connectivity (Fig. 2B) and structural between-module connectivity (Fig. 4B), the patient and control participant values were virtually identical, suggesting that the protocol differences did not appear to create a substantial baseline difference between the patient and controls.

4.2. Conclusions

Functional and structural brain connectivity, for this patient, demonstrated substantial neuroplasticity in response to amputation and bilateral hand transplantation. At the preoperative baseline, relative to controls, the patient exhibited higher within-module functional connectivity, for both SMN and non-SMN modules, and higher within-module structural connectivity for the SMN module. These differences, measured preoperatively, suggest a change in brain organization in response to amputation. Across 1.5 years postoperatively, the within-module functional connectivity decreased towards the control participants' values, particularly for hand-related nodes within the SMN module, reflecting a return to a more canonical functional organization. The patient's structural connectivity values, in contrast, relatively constant postoperatively. However, some evidence also suggested that structural connectivity supported functional within-module connectivity at each testing session.

Funding

This work was supported by National Institutes of Health (NIH) research grants R01 AG039684 (DJM), R56 AG052576 (DJM), a grant from the Department of Defense W81XWH-12-2-0058 (LCC), and the Duke Health Scholar Award (LCC).

The data generated during and/or analyzed during the current study are not publicly available but will be made available upon reasonable request, based on approval from the requesting researcher's local ethics committee. Depending on the nature of the request, a formal data-sharing agreement may be required.

CRediT authorship contribution statement

David J. Madden: Writing – review & editing, Writing – original draft, Methodology, Funding acquisition, Formal analysis, Data curation, Conceptualization. **Jenna L. Merenstein:** Writing – review & editing, Writing – original draft, Software, Methodology, Formal analysis, Data curation, Conceptualization. **Todd B. Harshbarger:** Writing – review & editing, Software, Methodology, Data curation, Conceptualization. **Linda C. Cendales:** Writing – review & editing, Supervision, Methodology, Funding acquisition, Data curation, Conceptualization.

Declaration of competing interest

The authors report no conflicts of interest.

Data availability

Data will be made available from a reasonable request, with approval from the requesting researcher's IRB. Depending on the nature of the request, a formal data-sharing agreement may be required.

Acknowledgments

We are grateful to Tina Zhao, Hollie Mullin, and the Duke VCA Program team, for their assistance, and to the patient and their family for their generosity and willingness to participate in this research.

Appendix A. Supplementary data

Supplementary data to this article can be found online at https://doi.org/10.1016/j.ynirp.2024.100222.

References

Alakörkkö, T., Saarimäki, H., Glerean, E., Saramäki, J., Korhonen, O., 2017. Effects of spatial smoothing on functional brain networks. Eur. J. Neurosci. 46, 2471–2480. https://doi.org/10.1111/ejn.13717.

Avants, B.B., Tustison, N.J., Song, G., Cook, P.A., Klein, A., Gee, J.C., 2011. A reproducible evaluation of ANTs similarity metric performance in brain image registration. Neuroimage 54, 2033–2044. https://doi.org/10.1016/j.neuroimage.2010.09.025.

Bastiani, M., Cottaar, M., Fitzgibbon, S.P., Suri, S., Alfaro-Almagro, F., Sotiropoulos, S.N., Jbabdi, S., Andersson, J.L.R., 2019. Automated quality control for within and between studies diffusion MRI data using a non-parametric framework for movement and distortion correction. Neuroimage 184, 801–812. https://doi.org/10.1016/j.neuroimage.2018.09.073.

Blondel, V.D., Guillaume, J.-L., Lambiotte, R., Lefebvre, E., 2008. Fast unfolding of communities in large networks. J. Stat. Mech. Theor. Exp. 2008, P10008. https://doi.org/10.1088/1742-5468/2008/10/p10008.

Bramati, I.E., Rodrigues, E.C., Simões, E.L., Melo, B., Höfle, S., Moll, J., Lent, R., Tovar-Moll, F., 2019. Lower limb amputees undergo long-distance plasticity in sensorimotor functional connectivity. Sci. Rep. 9, 2518. https://doi.org/10.1038/s41598-019-39696-z.

Brenneis, C., Loscher, W.N., Egger, K.E., Benke, T., Schocke, M., Gabl, M.F., Wechselberger, G., Felber, S., Pechlaner, S., Margreiter, R., Piza-Katzer, H., Poewe, W., 2005. Cortical motor activation patterns following hand transplantation and replantation. J. Hand. Surg. Eur. 30, 530–533. https://doi.org/10.1016/j.jhsb.2005.05.012.

Bullmore, E., Sporns, O., 2009. Complex brain networks: graph theoretical analysis of structural and functional systems. Nat. Rev. Neurosci. 10, 186–198. https://doi.org/10.1038/nrn2575.

Buonomano, D.V., Merzenich, M.M., 1998. Cortical plasticity: from synapses to maps. Annu. Rev. Neurosci. 21, 149–186. https://doi.org/10.1146/annurev.neuro.21.1.149.

Cendales, L.C., Kanitakis, J., Schneeberger, S., Burns, C., Ruiz, P., Landin, L., Remmelink, M., Hewitt, C.W., Landgren, T., Lyons, B., Drachenberg, C.B., Solez, K., Kirk, A.D., Kleiner, D.E., Racusen, L., 2008. The Banff 2007 working classification of skin-containing composite tissue allograft pathology. Am. J. Transplant. 8, 1396–1400. https://doi.org/10.1111/j.1600-6143.2008.02243.x.

Cendales, L.C., Rahmel, A., Pruett, T.L., 2012. Allocation of vascularized composite allografts: what is it? Transplantation 93, 1086–1087. https://doi.org/10.1097/TP.0b013e31824b073f.

Cendales, L.C., Ruch, D.S., Cardones, A.R., Potter, G., Dooley, J., Dore, D., Orr, J., Ruskin, G., Song, M., Chen, D.F., Selim, M.A., Kirk, A.D., 2018. De novo belatacept in clinical vascularized composite allotransplantation. Am. J. Transplant. 18, 1804–1809. https://doi.org/10.1111/ajt.14910.

Ciric, R., Wolf, D.H., Power, J.D., Roalf, D.R., Baum, G.L., Ruparel, K., Shinohara, R.T., Elliott, M.A., Eickhoff, S.B., Davatzikos, C., Gur, R.C., Gur, R.E., Bassett, D.S., Satterthwaite, T.D., 2017. Benchmarking of participant-level confound regression strategies for the control of motion artifact in studies of functional connectivity. Neuroimage 154, 174–187. https://doi.org/10.1016/j.neuroimage.2017.03.020.

Clayden, J.D., 2013. Imaging connectivity: MRI and the structural networks of the brain. Funct. Neurol. 28, 197–203.

Cox, R.W., 1996. AFNI: software for analysis and visualization of functional magnetic resonance neuroimages. Comput. Biomed. Res. 29, 162–173. https://doi.org/10.1006/cbmr.1996.0014.

Damoiseaux, J.S., Greicius, M.D., 2009. Greater than the sum of its parts: a review of studies combining structural connectivity and resting-state functional connectivity. Brain Struct. Funct. 213, 525–533. https://doi.org/10.1007/s00429-009-0208-6.

Dubernard, J.-M., Owen, E., Herzberg, G., Lanzetta, M., Martin, X., Kapila, H., Dawahra, M., Hakim, N.S., 1999. Human hand allograft: report on first 6 months. Lancet 353, 1315–1320. https://doi.org/10.1016/S0140-6736(99)02062-0.

Dunnett, C.W., 1955. A multiple comparison procedure for comparing several treatments with a control. J. Am. Stat. Assoc. 50, 1096–1121. https://doi.org/10.2307/2281208.

Esteban, O., Markiewicz, C.J., Blair, R.W., Moodie, C.A., Isik, A.I., Erramuzpe, A., Kent, J. D., Goncalves, M., DuPre, E., Snyder, M., Oya, H., Ghosh, S.S., Wright, J., Durnez, J., Poldrack, R.A., Gorgolewski, K.J., 2019. fMRIPrep: a robust preprocessing pipeline for functional MRI. Nat. Methods 16, 111–116. https://doi.org/10.1038/s41592-018-0235-4.

Fan, L., Li, H., Zhuo, J., Zhang, Y., Wang, J., Chen, L., Yang, Z., Chu, C., Xie, S., Laird, A. R., Fox, P.T., Eickhoff, S.B., Yu, C., Jiang, T., 2016. The human brainnetome atlas: a new brain atlas based on connectional architecture. Cerebr. Cortex 26, 3508–3526. https://doi.org/10.1093/cercor/bhw157.

Feldman, D.E., Brecht, M., 2005. Map plasticity in somatosensory cortex. Science 310, 810–815. https://doi.org/10.1126/science.1115807.

Flor, H., Elbert, T., Knecht, S., Wienbruch, C., Pantev, C., Birbaumer, N., Larbig, W., Taub, E., 1995. Phantom-limb pain as a perceptual correlate of cortical reorganization following arm amputation. Nature 375, 482–484. https://doi.org/10.1038/375482a0.

Folstein, M.F., Folstein, S.E., McHugh, P.R., 1975. "Mini-mental state." A practical method for grading the cognitive state of patients for the clinician. J. Psychiatr. Res. 12, 189–198. https://doi.org/10.1016/0022-3956(75)90026-6.

Fornito, A., Zalesky, A., Bullmore, E., 2010. Network scaling effects in graph analytic studies of human resting-state fMRI data. Front. Syst. Neurosci. 4. https://doi.org/10.3389/fnsys.2010.00022.

Frey, S.H., Bogdanov, S., Smith, J.C., Watrous, S., Breidenbach, W.C., 2008. Chronically deafferented sensory cortex recovers a grossly typical organization after allogenic hand transplantation. Curr. Biol. 18, 1530–1534. https://doi.org/10.1016/j.cub.2008.08.051.

Gargouri, F., Kallel, F., Delphine, S., Ben Hamida, A., Lehéricy, S., Valabregue, R., 2018. The influence of preprocessing steps on graph theory measures derived from resting state fMRI. Front. Comput. Neurosci. 12. https://doi.org/10.3389/fncom.2018.00008.

Giraux, P., Sirigu, A., Schneider, F., Dubernard, J.M., 2001. Cortical reorganization in motor cortex after graft of both hands. Nat. Neurosci. 4, 691–692. https://doi.org/10.1038/89472.

Gordon, E.M., Laumann, T.O., Adeyemo, B., Huckins, J.F., Kelley, W.M., Petersen, S.E., 2014. Generation and evaluation of a cortical area parcellation from resting-state correlations. Cerebr. Cortex 26, 288–303. https://doi.org/10.1093/cercor/bhu239.

Greve, D.N., Fischl, B., 2009. Accurate and robust brain image alignment using boundary-based registration. Neuroimage 48, 63. https://doi.org/10.1016/J.NEUROIMAGE.2009.06.060, 63.

Hagmann, P., Cammoun, L., Gigandet, X., Meuli, R., Honey, C.J., Wedeen, V.J., Sporns, O., 2008. Mapping the structural core of human cerebral cortex. PLoS Biol. 6, e159. https://doi.org/10.1371/journal.pbio.0060159.

Hernandez-Castillo, C.R., Aguilar-Castaneda, E., Iglesias, M., Fernandez-Ruiz, J., 2016. Motor and sensory cortical reorganization after bilateral forearm transplantation: four-year follow-up fMRI case study. Magn. Reson. Imaging 34, 541–544. https://doi.org/10.1016/j.mri.2015.12.025.

Hernandez-Castillo, C.R., Diedrichsen, J., Aguilar-Castañeda, E., Iglesias, M., 2018. Decoupling between the hand territory and the default mode network after bilateral arm transplantation: four-year follow-up case study. Brain Imaging Behav. 12, 296–302. https://doi.org/10.1007/s11682-017-9683-1.

Hinkle, D.E., Wiersma, W., Jurs, S.G., 1988. Applied Statistics for the Behavioral Sciences, second ed. Houghton Mifflin, Boston.

Honey, C.J., Sporns, O., Cammoun, L., Gigandet, X., Thiran, J.P., Meuli, R., Hagmann, P., 2009. Predicting human resting-state functional connectivity from structural connectivity. Proc. Natl. Acad. Sci. U.S.A. 106, 2035–2040. https://doi.org/10.1073/pnas.0811168106.

Ji, J.L., Spronk, M., Kulkarni, K., Repovs, G., Anticevic, A., Cole, M.W., 2019. Mapping the human brain's cortical-subcortical functional network organization. Neuroimage 185, 35–57. https://doi.org/10.1016/j.neuroimage.2018.10.006.

Lancichinetti, A., Fortunato, S., 2012. Consensus clustering in complex networks. Sci. Rep. 2, 336. https://doi.org/10.1038/srep00336.

Li, X., Bianchini Esper, N., Ai, L., Giavasis, S., Jin, H., Feczko, E., Xu, T., Clucas, J., Franco, A., Sólon Heinsfeld, A., Adebimpe, A., Vogelstein, J.T., Yan, C.-G., Esteban, O., Poldrack, R.A., Craddock, C., Fair, D., Satterthwaite, T., Kiar, G., Milham, M.P., 2024. Moving beyond processing- and analysis-related variation in resting-state functional brain imaging. Nat. Human Behav. https://doi.org/10.1038/s41562-024-01942-4.

Lotze, M., Flor, H., Grodd, W., Larbig, W., Birbaumer, N., 2001. Phantom movements and pain an fMRI study in upper limb amputees. Brain 124, 2268–2277. https://doi.org/10.1093/brain/124.11.2268.

Luppi, A.I., Gellersen, H.M., Liu, Z.-Q., Peattie, A.R.D., Manktelow, A.E., Adapa, R., Owen, A.M., Naci, L., Menon, D.K., Dimitriadis, S.I., Stamatakis, E.A., 2024. Systematic evaluation of fMRI data-processing pipelines for consistent functional connectomics. Nat. Commun. 15, 4745. https://doi.org/10.1038/s41467-024-48781-5.

MacKay, B.J., Nacke, E., Posner, M., 2014. Hand transplantation: a review. Bull. Hosp. Jt. Dis. 72, 76–88.

Madden, D.J., Melton, M.S., Jain, S., Cook, A.D., Browndyke, J.N., Harshbarger, T.B., Cendales, L.C., 2019. Neural activation for actual and imagined movement following unilateral hand transplantation: a case study. Neurocase 25, 225–234. https://doi.org/10.1080/13554794.2019.1667398.

Madden, D.J., Merenstein, J.L., Mullin, H.A., Jain, S., Rudolph, M.D., Cohen, J.R., 2024. Age-related differences in resting-state, task-related, and structural brain connectivity: graph theoretical analyses and visual search performance. Brain Struct. Funct. 229, 1533–1559. https://doi.org/10.1007/s00429-024-02807-2.

Makin, T.R., Bensmaia, S.J., 2017. Stability of sensory topographies in adult cortex. Trends Cognit. Sci. 21, 195–204. https://doi.org/10.1016/j.tics.2017.01.002.

Makin, T.R., Filippini, N., Duff, E.P., Henderson Slater, D., Tracey, I., Johansen-Berg, H., 2015a. Network-level reorganisation of functional connectivity following arm amputation. Neuroimage 114, 217–225. https://doi.org/10.1016/j.neuroimage.2015.02.067.

Makin, T.R., Scholz, J., Filippini, N., Henderson Slater, D., Tracey, I., Johansen-Berg, H., 2013. Phantom pain is associated with preserved structure and function in the former hand area. Nat. Commun. 4, 1570. https://doi.org/10.1038/ncomms2571.

Makin, T.R., Scholz, J., Henderson Slater, D., Johansen-Berg, H., Tracey, I., 2015b. Reassessing cortical reorganization in the primary sensorimotor cortex following arm amputation. Brain 138, 2140–2146. https://doi.org/10.1093/brain/awv161.

Merenstein, J.L., Howard, C.M., Madden, D.J., 2023a. Aging and neuroplasticity. Reference Module in Neuroscience and Biobehavioral Psychology. https://doi.org/10.1016/B978-0-12-820480-1.00041-3.

Merenstein, J.L., Mullin, H.A., Madden, D.J., 2023b. Age-related differences in frontoparietal activation for target and distractor singletons during visual search. Atten. Percept. Psychophys. 85, 749–768. https://doi.org/10.3758/s13414-022-02640-x.

Meyer, V.E., 1991. Major limb replantation revascularization. In: Meyer, V.E., Black, M. J.M. (Eds.), Microsurgical Procedures. Churchill Livingstone, Edinburgh, pp. 36–68.

Murphy, K., Fox, M.D., 2017. Towards a consensus regarding global signal regression for resting state functional connectivity MRI. Neuroimage 154, 169–173. https://doi.org/10.1016/j.neuroimage.2016.11.052.

Nakamura, T., Hillary, F.G., Biswal, B.B., 2009. Resting network plasticity following brain injury. PLoS One 4, e8220. https://doi.org/10.1371/journal.pone.0008220.

Neugroschl, C., Denolin, V., Schuind, F., Van Holder, C., David, P., Baleriaux, D., Metens, T., 2005. Functional MRI activation of somatosensory and motor cortices in a hand-grafted patient with early clinical sensorimotor recovery. Eur. Radiol. 15, 1806–1814. https://doi.org/10.1007/s00330-005-2763-4.

Parkes, L., Fulcher, B., Yücel, M., Fornito, A., 2018. An evaluation of the efficacy, reliability, and sensitivity of motion correction strategies for resting-state functional MRI. Neuroimage 171, 415–436. https://doi.org/10.1016/j.neuroimage.2017.12.073.

Petruzzo, P., Badet, L., Gazarian, A., Lanzetta, M., Parmentier, H., Kanitakis, J., Sirigu, A., Martin, X., Dubernard, J.M., 2006. Bilateral hand transplantation: six years after the first case. Am. J. Transplant. 6, 1718–1724. https://doi.org/10.1111/j.1600-6143.2006.01369.x.

Philip, B.A., Valyear, K.F., Cirstea, C.M., Baune, N.A., Kaufman, C., Frey, S.H., 2022. Changes in primary somatosensory cortex following allogeneic hand transplantation or autogenic hand replantation. Front. Neuroimaging 1. https://doi.org/10.3389/fnimg.2022.919694.

Poldrack, R.A., 2000. Imaging brain plasticity: conceptual and methodological issues–a theoretical review. Neuroimage 12, 1–13. https://doi.org/10.1006/nimg.2000.0596.

Power, J.D., Barnes, K.A., Snyder, A.Z., Schlaggar, B.L., Petersen, S.E., 2012. Spurious but systematic correlations in functional connectivity MRI networks arise from subject motion. Neuroimage 59, 2142–2154. https://doi.org/10.1016/j.neuroimage.2011.10.018.

Power, J.D., Cohen, A.L., Nelson, S.M., Wig, G.S., Barnes, K.A., Church, J.A., Vogel, A.C., Laumann, T.O., Miezin, F.M., Schlaggar, B.L., Petersen, S.E., 2011. Functional network organization of the human brain. Neuron 72, 665–678. https://doi.org/10.1016/j.neuron.2011.09.006.

Power, J.D., Mitra, A., Laumann, T.O., Snyder, A.Z., Schlaggar, B.L., Petersen, S.E., 2014. Methods to detect, characterize, and remove motion artifact in resting state fMRI. Neuroimage 84, 320–341. https://doi.org/10.1016/j.neuroimage.2013.08.048.

Rubinov, M., Sporns, O., 2010. Complex network measures of brain connectivity: uses and interpretations. Neuroimage 52, 1059–1069. https://doi.org/10.1016/j.neuroimage.2009.10.003.

Rubinov, M., Sporns, O., 2011. Weight-conserving characterization of complex functional brain networks. Neuroimage 56, 2068–2079. https://doi.org/10.1016/j.neuroimage.2011.03.069.

Satterthwaite, T.D., Elliott, M.A., Gerraty, R.T., Ruparel, K., Loughead, J., Calkins, M.E., Eickhoff, S.B., Hakonarson, H., Gur, R.C., Gur, R.E., Wolf, D.H., 2013. An improved framework for confound regression and filtering for control of motion artifact in the preprocessing of resting-state functional connectivity data. Neuroimage 64, 240–256. https://doi.org/10.1016/j.neuroimage.2012.08.052.

Shores, J.T., Brandacher, G., Schneeberger, S., Gorantla, V.S., Lee, W.P., 2010. Composite tissue allotransplantation: hand transplantation and beyond. J. Am. Acad. Orthop. Surg. 18, 127–131.

Shores, J.T., Malek, V., Lee, W.P.A., Brandacher, G., 2017. Outcomes after hand and upper extremity transplantation. J. Mater. Sci. Mater. Med. 28, 72. https://doi.org/10.1007/s10856-017-5880-0.

Simoes, E.L., Bramati, I., Rodrigues, E., Franzoi, A., Moll, J., Lent, R., Tovar-Moll, F., 2012. Functional expansion of sensorimotor representation and structural reorganization of callosal connections in lower limb amputees. J. Neurosci. 32, 3211–3220. https://doi.org/10.1523/JNEUROSCI.4592-11.2012.

Smith, R.E., Tournier, J.-D., Calamante, F., Connelly, A., 2012. Anatomically-constrained tractography: improved diffusion MRI streamlines tractography through effective use of anatomical information. Neuroimage 62, 1924–1938. https://doi.org/10.1016/j.neuroimage.2012.06.005.

Smith, R.E., Tournier, J.-D., Calamante, F., Connelly, A., 2015. The effects of SIFT on the reproducibility and biological accuracy of the structural connectome. Neuroimage 104, 253–265. https://doi.org/10.1016/j.neuroimage.2014.10.004.

Smith, R.E., Tournier, J.D., Calamante, F., Connelly, A., 2013. SIFT: spherical-deconvolution informed filtering of tractograms. Neuroimage 67, 298–312. https://doi.org/10.1016/j.neuroimage.2012.11.049.

Smith, S.M., Jenkinson, M., Woolrich, M.W., Beckmann, C.F., Behrens, T.E., Johansen-Berg, H., Bannister, P.R., De Luca, M., Drobnjak, I., Flitney, D.E., Niazy, R.K., Saunders, J., Vickers, J., Zhang, Y., De Stefano, N., Brady, J.M., Matthews, P.M., 2004. Advances in functional and structural MR image analysis and implementation as FSL. Neuroimage 23 (Suppl. 1), S208–S219. https://doi.org/10.1016/j.neuroimage.2004.07.051.

Sporns, O., 2011. The human connectome: a complex network. Ann. N. Y. Acad. Sci. 1224, 109–125. https://doi.org/10.1111/j.1749-6632.2010.05888.x.

Sporns, O., Betzel, R.F., 2016. Modular brain networks. Annu. Rev. Psychol. 67, 613–640. https://doi.org/10.1146/annurev-psych-122414-033634.

Taub, E., Uswatte, G., Elbert, T., 2002. New treatments in neurorehabilitation founded on basic research. Nat. Rev. Neurosci. 3, 228–236. https://doi.org/10.1038/nrn754.

Tournier, J.D., Smith, R., Raffelt, D., Tabbara, R., Dhollander, T., Pietsch, M., Christiaens, D., Jeurissen, B., Yeh, C.-H., Connelly, A., 2019. MRtrix3: a fast, flexible and open software framework for medical image processing and visualisation. Neuroimage 202, 116137. https://doi.org/10.1016/j.neuroimage.2019.116137.

Treiber, J.M., White, N.S., Steed, T.C., Bartsch, H., Holland, D., Farid, N., McDonald, C. R., Carter, B.S., Dale, A.M., Chen, C.C., 2016. Characterization and correction of geometric distortions in 814 diffusion weighted images. PLoS One 11, e0152472. https://doi.org/10.1371/journal.pone.0152472.

Valyear, K.F., Mattos, D., Philip, B.A., Kaufman, C., Frey, S.H., 2019. Grasping with a new hand: improved performance and normalized grasp-selective brain responses despite persistent functional changes in primary motor cortex and low-level sensory and motor impairments. Neuroimage 190, 275–288. https://doi.org/10.1016/j.neuroimage.2017.09.052.

Valyear, K.F., Philip, B.A., Cirstea, C.M., Chen, P.-W., Baune, N.A., Marchal, N., Frey, S. H., 2020. Interhemispheric transfer of post-amputation cortical plasticity within the human somatosensory cortex. Neuroimage 206, 116291. https://doi.org/10.1016/j.neuroimage.2019.116291.

Wells, M.W., Rampazzo, A., Papay, F., Gharb, B.B., 2022. Two decades of hand transplantation: a systematic review of outcomes. Ann. Plast. Surg. 88, 335–344. https://doi.org/10.1097/sap.0000000000003056.

Ye, C., Zhuo, J., Gullapalli, R.P., Prince, J.L., 2016. Estimation of fiber orientations using neighborhood information. Med. Image Anal. 32, 243–256. https://doi.org/10.1016/j.media.2016.05.008.

Yeh, C.H., Jones, D.K., Liang, X., Descoteaux, M., Connelly, A., 2021. Mapping structural connectivity using diffusion MRI: challenges and opportunities. J. Magn. Reson. Imag. 53, 1666–1682. https://doi.org/10.1002/jmri.27188.

Yeo, B.T., Krienen, F.M., Sepulcre, J., Sabuncu, M.R., Lashkari, D., Hollinshead, M., Roffman, J.L., Smoller, J.W., Zöllei, L., Polimeni, J.R., Fisch, B., Liu, H., Buckner, R. L., 2011. The organization of the human cerebral cortex estimated by intrinsic functional connectivity. J. Neurophysiol. 106, 1125–1165. https://doi.org/10.1152/jn.00338.2011.